ORIGINAL ARTICLE

Investigation of local load effect on damping characteristics of synchronous generator using transfer-function block-diagram model

Pichai Aree

Abstract

Aree, P.
Investigation of local load effect on damping characteristics of synchronous generator using transfer-function block-diagram model
Songklanakarin J. Sci. Technol., 2005, 27(4) : 827-838

The transfer-function block-diagram model of single-machine infinite-bus power system has been a popular analytical tool amongst power engineers for explaining and assessing synchronous generator dynamic behaviors. In previous studies, the effects of local load together with damper circuit on generator damping have not yet been addressed because neither of them was integrated into this model. Since the model only accounts for the generator main field circuit, it may not always yield a realistic damping assessment due to lack of damper circuit representation. This paper presents an extended transfer-function block-diagram model, which includes one of the *q*-axis damper circuits as well as local load. This allows a more realistic investigation of the local load effect on the generator damping. The extended model is applied to assess the generator dynamic performance. The results show that the damping power components mostly derived from the *q*-axis damper and the field circuits can be improved according to the local load. The frequency response method is employed to carry out the fundamental analysis.

Key words : power system stability, damping, local load

Ph.D.(Electrical Engineering), Asst. Prof., Department of Electrical Engineering, Faculty of Engineering Thammasat, University, Klong Luang, Pathum Thani, 12120 Thailand.
E-mail: apichai@engr.tu.ac.th
Received, 26 July 2004 Accepted, 8 November 2004

บทคัดย่อ

พิชัย อารีย์

การศึกษาผลกระทบของโลดอลโหลดต่อคุณลักษณะความหน่วงของเครื่องกำเนิดไฟฟ้าซิงโครนัสโดยใช้แบบจำลองแผนภาพกล่องฟังก์ชั่นถ่ายโอน

ว. สงขลานครินทร์ วทท. 2548 27(4) : 827-838

แบบจำลองของระบบไฟฟ้ากำลังในรูปของแบบจำลองแผนภาพกล่องฟังก์ชันถ่ายโอน (transfer-function block-diagram model) เป็นที่นิยมในการอธิบายและวิเคราะห์พฤติกรรมทางพลวัตของเครื่องกำเนิดไฟฟ้าซิงโครนัส (synchronous generator) แต่การศึกษาแบบจำลองที่ผ่านมาได้พิจารณาชุดขดลวดสนาม (field winding) ของเครื่องกำเนิดไฟฟ้าเท่านั้น มิได้พิจารณาชุดขดลวดหน่วง (damper winding) และโลดอลโหลด (local load) ร่วมกันในการวิเคราะห์ความหน่วงของเครื่องกำเนิดไฟฟ้า จึงทำให้ไม่สามารถวิเคราะห์ผลกระทบของโลดอลโหลดต่อคุณลักษณะความหน่วงของเครื่องกำเนิดไฟฟ้าได้อย่างถูกต้อง ดังนั้นการศึกษานี้จึงได้ปรับปรุงแบบจำลองของระบบไฟฟ้าโดยพิจารณาชุดขดลวดหน่วงในแกนขวาง (*q*-axis damper winding) ซึ่งแบบจำลองนี้ทำให้การวิเคราะห์ผลกระทบของโลดอลโหลดต่อค่าความหน่วงของเครื่องกำเนิดไฟฟ้าเป็นไปได้อย่างสมบูรณ์ จากการศึกษาโดยใช้วิธีตอบสนองทางความถี่ (frequency response method) พบว่าโลดอลโหลดสามารถเพิ่มความหน่วงให้กับเครื่องกำเนิดไฟฟ้าผ่านทางขดลวดหน่วงแกนขวาง และขดลวดสนาม

ภาควิชาวิศวกรรมไฟฟ้า คณะวิศวกรรมศาสตร์ มหาวิทยาลัยธรรมศาสตร์ อำเภอคลองหลวง จังหวัดปทุมธานี 12121

The transfer-function block diagram model of single-machine infinite-bus power system (Demello *et al*., 1969; Anderson, 1993; Saidy *et al*., 1994; Padiyar, 1995) has provided the basis for excellent explanation of fundamental dynamic characteristics of synchronous generator. It has been used amongst power engineers for many years to design the control equipments such as automatic voltage regulator (AVR) and power system stabilizer (PSS). The model yields a great physical insight into how AVR and PSS enhance power system stability.

The transfer-function block-diagram models were advanced to incorporate an electric local load (El-Sherbiny *et al*., 1973; Yu, 1983; Saccomanno, 2003). The constant impedance load model was conventionally used to represent the local load. These block-diagram models help to demonstrate the effect of the local load on stability of synchronous generator. However, reliability of the models has been brought into question because they only take into account the generator field circuit. Hence, use of a higher-order block-diagram model (Saidy *et al*., 1994) has been realized by including the *d* and *q*-axis damper circuits to obtain the realistic damping assessment of synchronous generator (Saidy *et al*., 1994). However, in this model, the effect of the local load has not yet been taken into consideration.

In this paper, the transfer-function block-diagram model (Saidy *et al*., 1994) has been extended to incorporate the constant impedance local load and the damper circuit representation. According to the previous studies (Saidy *et al*., 1994; Aree *et al*., 1999), one of the *q*-axis damper circuits is essentially added, in addition to the field winding, to provide the system realistic damping. The block-diagram model provides an insightful analysis of how the local load affects the damping characteristics of synchronous generator through the field and *q*-axis damper circuits. Moreover, this model is applied to demonstrate the local load effect on dynamic performance of the generator under voltage regulator. The analysis is carried out using the frequency response method.

1. System and transfer-function block-diagram representation

In order to investigate the fundamental effect of local load on damping of the synchronous generator, the study system used by Yu (1983) is modified to include the representation of the *q*-axis damper circuit. This system is shown in Figure 1. It consists of one synchronous generator in connection with an infinite bus through the tie line system. It should be noted that since the main objective of this paper is to gain a fundamental knowledge of interaction between the generator and the local load, this system is suitable for this study. The small-signal model that represents the system under study is derived using the non-linear differential and algebraic equations (Arrilaga *et al*., 1990), given by (A-1)-(A-8) in Appendix A. After completing the derivation process presented in Appendix A, the small-signal linearized transfer functions in s domain are expressed as,

$$s\Delta\delta = \omega_s \Delta\omega_r \tag{1}$$

$$2Hs\Delta\omega_r = \Delta P_m - \Delta P_e - K_D \Delta\omega_r \tag{2}$$

$$(1 + K_{3q}\tau'_{do}s)\Delta E'_q = K_{3q}\Delta E_{fd} - K_{4q}\Delta\delta + K_{7q}\Delta E'_d \tag{3}$$

$$(1 + K_{3d}\tau'_{qo}s)\Delta E'_d = -K_{4d}\Delta\delta - K_{7d}\Delta E'_q \tag{4}$$

$$\Delta P_e = K_1\Delta\delta + K_{2d}\Delta E'_d + K_{2q}\Delta E'_q \tag{5}$$

$$\Delta E_t = K_5\Delta\delta + K_{6d}\Delta E'_d + K_{6q}\Delta E'_q \tag{6}$$

The system *K*-coefficients are listed by (A-13)-(A-27) in Appendix A. Equations (1)-(6) comprehensively describe the small-signal dynamics of the study system. By suitably combining (1)-(6), the linearized transfer function in the form of block diagram is displayed inside the dotted-line block of Figure 2. The local load affects the generator dynamic characteristics through all the *K*-coefficients, which are a function of load conductance (G) and susceptance (B). Furthermore, the local load gives rise to the additional coefficients K_{7d} and K_{7q}, which exist in addition to the *K*-coefficients presented in the block-diagram model developed by Demello (1969), Yu (1983), Saidy *et al*., (1994). The dynamic interactions between the generator flux linkages ($\Delta E'_q$ and $\Delta E'_d$) in the *d* and *q*-axes take place through the K_{7q} and K_{7d} branches. According to (A-15) and (A-19), the coefficients K_{7q} and K_{7d} will not appear in the block-diagram model, if the local load is not incorporated. Because the local load influences the dynamic characteristics of the generator flux linkages $\Delta E'_q$ and $\Delta E'_d$ with regard to its conductance and susceptance, the damping power components of the electrical powers P_{fd} and P_q, mainly derived from the field and *q*-axis damper circuits, respectively, are affected. The investigations into effect of the local load on the generator damping characteristics are carried out in the next section.

2. Effect of local load on damping characteristics of field and damper circuits

In this section, the effects of the local load on generator damping over the relevant frequency range of 1-12 rad/s are investigated. The active power output of the generator is kept at 0.8 per unit (on 100MVA base), whether or not the local load is included into the system. The generator is equipped with AVR (K_a = 200, τ_a = 1 sec) and with

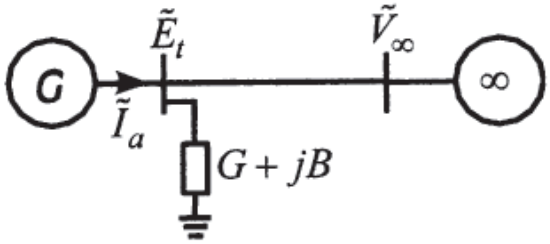

Figure 1. Synchronous generator with grid and local load.

no PSS. The generator initially has low damping due to its making use of the high tie-line reactance (0.6 pu) between the generator and infinite bus. It should be noted that the high value of the inter-connected tie causes degrading in the generator damping (Saidy *et al*., 1994). The generator and infinite-bus voltages are kept at 1.0 per unit. The generator and AVR parameters are given in Appendix B.

To gain an insight into the effect of the local load on generator damping characteristics through the *q*-axis damper and field circuits, the dynamic responses of electrical power P_q and P_{fd} due to the oscillation of rotor angle δ are entirely explored. A measure of contributions of both rotor circuits to synchronizing and damping powers is determined from the frequency responses of P_q/δ and P_{fd}/δ (Saidy *et al*., 1995), shown in Figure 3 and 4. These responses are plotted in the Nyquist form with an aid of the transfer-function block-diagram model in Figure 2. It should be noted from the Nyquist plots that the coordinate of P_q/δ and P_{fd}/δ in the δ direction (real axis) gives the synchronizing power component, and the coordinate in the ω direction (imaginary axis) gives the damping power component. The investigation is firstly carried out with no incorporation of the local load. In Figure 3, the response of P_q/δ covers the second quadrant along the positive ω direction in the δ- ω plane. This result indicates that the damping contribution derived from the *q*-axis damper circuit is naturally positive over an entire oscillation frequency. On the other hand, the response of P_{fd}/δ in Figure 4 covers the third and fourth quadrants along the negative ω direction between 3.9-8.0 rad/s. Thus, the field circuit in connection with the high-gain AVR injects negative damping into the system throughout this frequency range. The combined responses of P_{fd}/δ and P_q/δ, plotted in Figure 5, are used to explore the overall damping characteristics of the system, which are derived from both field and damper circuits. From these responses, the capability of the *q*-axis damper circuit to enhance the system damping can be seen. For example, as compared with the response of P_{fd}/δ (dotted line in Figure 4), the combined response (dotted line in Figure 5) has smaller magnitude and narrower range of the oscillation frequencies that covers the third and fourth quadrants. This result is due to the *q*-axis damper circuit, which aids alleviation of the field negative damping effect

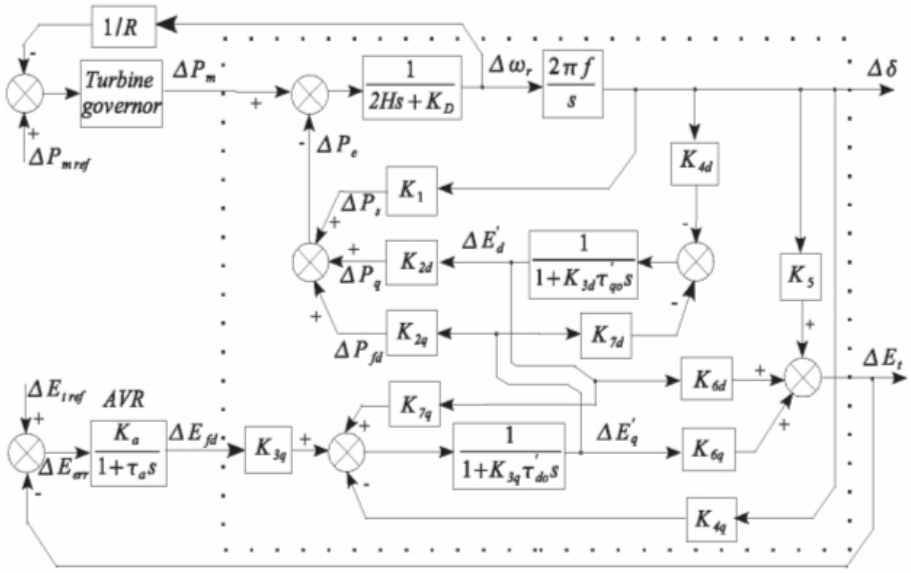

Figure 2. Transfer-function block-diagram model of the study system.

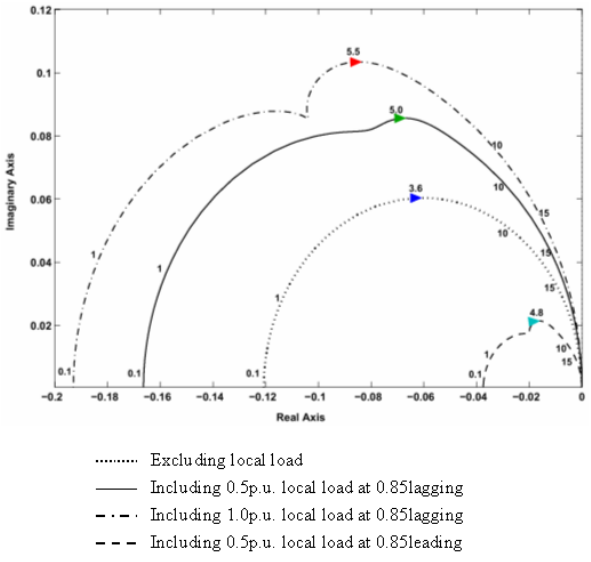

Figure 3. Frequency response of $P_q/\ \delta$

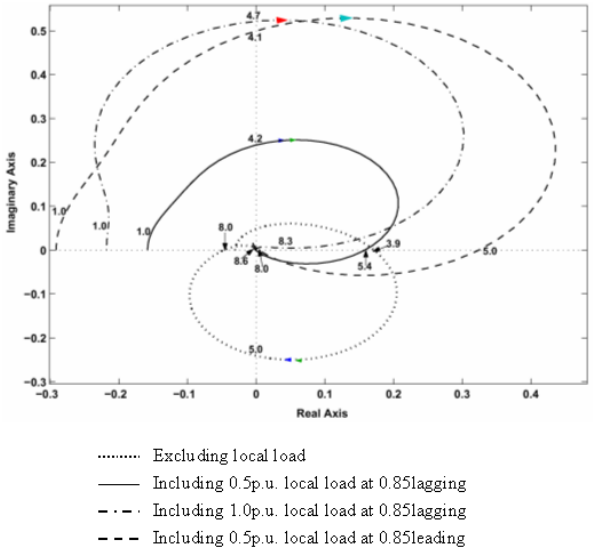

Figure 4. Frequency response of $P_{fd}/\ \delta$

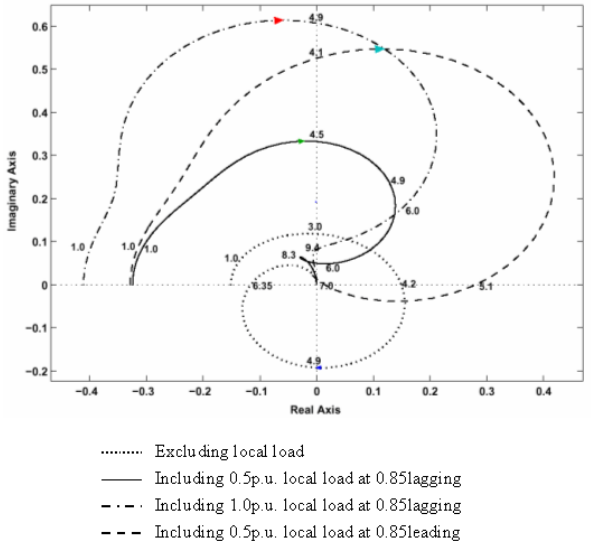

Figure 5. Combined frequency responses of $P_{fd}/\ \delta$ and $P_q/\ \delta$

according to the AVR.

Next, when the local load of 0.5 pu active power demand at typical 0.85 lagging condition is incorporated, the response of $P_{fd}/\ \delta$ that expands into the third and fourth quadrants is significantly dropped, as displayed in Figure 4. This consequence indicates a great reduction of the negative damping contribution from the field winding. In addition, the damping contribution from the *q*-axis damper circuit is greatly increased through a significant increase of the $P_q/\ \delta$ response, shown in Figure 3. The *q*-axis damper counteracts the field negative damping effect. Therefore, the overall damping is positive. This stable phenomenon can be observed through the total shifting of the combined response (solid line in Figure 5) into the first and second

quadrants.

The effects of the local load in relation to the changes in its active power consumption and power factor are further investigated. When the active power consumption of the local load is increased from 0.5 to 1.0 pu, the $P_q/\ \delta$ response is expanded along the positive ω direction into the second quadrant, as shown in Figure 3. Thus, more damping power contribution from the *q*-axis damper circuit is obtained. The damping contribution of the field circuit is also substantially increased over the entire oscillation frequencies since the response of $P_{fd}/\ \delta$ is shifted further into the first and second quadrants, as indicated in Figure 4. The combined response in Figure 5 also confirms a great damping improvement. On the other hand, when the power factor of the local load at 0.5 pu active power demand is changed from 0.85 lagging to 0.85 leading conditions, the frequency response of $P_q/\ \delta$ is dramatically contracted, as displayed in Figure 3. The damping derived from the *q*-axis damper circuit, thus, significantly declines over an entire oscillation frequency range. Moreover, the changing in the power factor causes the field winding to inject an undesired negative damping into the system at the frequency range between 5.0 and 8.6 rad/s, as shown in Figure 4. Hence, the generator becomes unstable due to lack of damping. The combined response in Figure 5 also confirms this unstable phenomenon.

3. Local load effect on generator closed-loop voltage control performance

In this section, the dynamic performances of the generator are assessed in the context of the closed-loop terminal voltage control using the open-loop frequency and time response, which are obtained with an aid of the transfer-function block-diagram model. The frequency responses, relating to the terminal voltage (E_t) and the error signal (E_{err}), are shown in Figure 6 and the time response

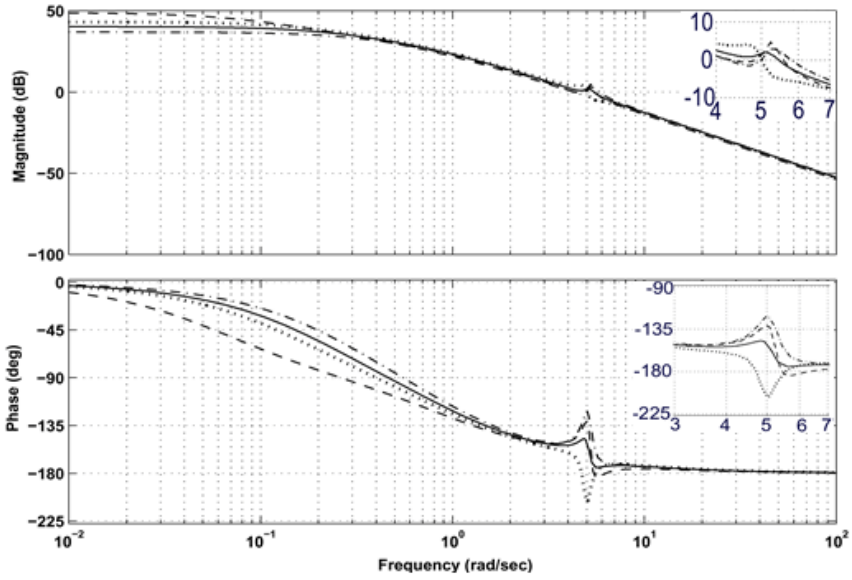

Figure 6. Frequency response of $E_t/\ E_{err}$

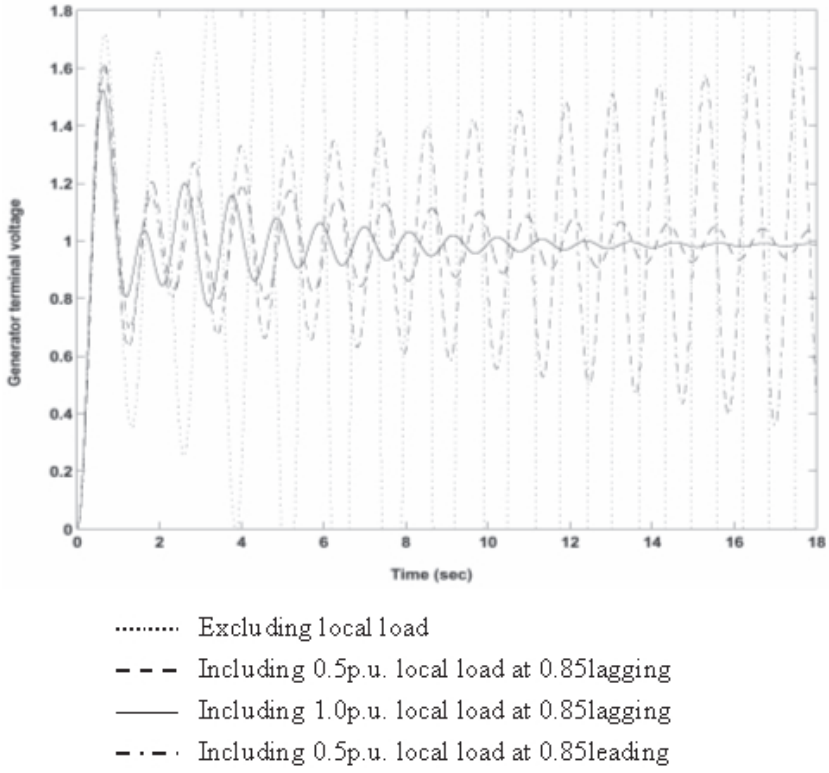

Figure 7. Time response of generator terminal voltage.

of terminal voltage is shown in Figure 7. When the generator has no local load, the phases and gains versus frequencies of E_t / E_{err} reveal the negative phase margin in connection to the highly marked switchback or dip characteristic at the oscillation frequency 5 rad/s. Hence, the generator becomces closed-loop unstable as seen through the undamped voltage response in Figure 7. On the other hand, when the local load of 0.5 pu active power demand at 0.85 lagging condition is incorporated, the phase versus frequency in Figure 6 shows considerable increases in the phase advance at the frequency around 5 rad/s. This phase advance reduces the switchback characteristic to improve the system phase margin. The generator, therefore, is stable. Moreover, as the level of load continues to increase from 0.5 to 1.0 pu, a greater phase advance of the frequency response is obtained. Hence, improving damping. The stable phenomena of the voltage control loop can be also seen through time response in Figure 7. The fact that the damping is enhanced due to an incorporation of the local load can be explained from the power transfer point of view. It has shown by Saidy *et al*., 1994 that the generator damping is depending upon the amount of the active power transfer from the generator to the infinite bus. The damping increases, when the power transfer decreases. For example, the generator without the local load delivers 0.8pu active power directly to the infinite bus. In the situation where the local load absorbs 0.5 pu active power, the generator power transfer is reduced from 0.8 to 0.3 per unit. Thus, the generator damping can be improved. On the contrary, when the power factor of the local load is changed from 0.85 lagging to 0.85 leading conditions at the same level of the active power demand (0.5pu), the gain and phase versus frequency in Figure 6 indicate the negative phase margin according to the pronounced switchback characteristic at the gain-crossover frequency (5.7 rad/s). Hence, the generator becomes unstable at this frequency due

to lack of damping. This unstable phenomenon with the growth of oscillation through terminal voltage response can be seen in Figure 7. It has been reported by Saidy *et al*., (1994) that the stability margin and the dynamic performance of the voltage control loop are deteriorated as the generator operating condition moves towards to leading condition. Because the changing in the load power factor from lagging to leading conditions causes the generator operating condition to become leading, the unstable closed-loop voltage control of the generator can occur.

Conclusions

A comprehensive transfer-function block-diagram model is presented in this paper. This model is far more realistic since the generator *q*-axis damper circuit is taken into account in addition to the field circuit. After the *q*-axis damper is incorporated, the extended block-diagram model shows the complete dynamic interaction, which mainly takes place between *q*-axis damper and the field flux linkages. The model is used to demonstrate a great influence of the local load on the damping characteristics of the individual *q*-axis damper and field circuits. With regard to the constant impedance local load operated at typical lagging power factor, the damping power contributions, derived from both *q*-axis damper and field circuits, are increased. The dynamic performance of the closed-loop voltage control is also improved through a reduction of the switchback characteristic. However, the damping contributions greatly decline, when the power factor of the local load is moved towards to the leading condition. In conclusion, an incorporation of the *q*-axis damper circuit yields realistic investigation of the local load effect on the generator damping characteristics. Without the representation of the *q*-axis damper circuit, the complete damping characteristics of synchronous generator cannot be captured.

Acknowledgement

The work described in this paper was sponsored by the Faculty of Engineering Research Center under grant number 010/2545-2546.

References

Anderson, P.M. and Fouad, A.A. 1993. Power System Control and Stability, IEEE Press, New York.

Aree, P. and Acha, E. 1999. Block diagram model for fundamental studies of a synchronous generator static var compensator system. IEE Proc. Gener. Transm. Distrib., 146: 507-514.

Arrillaga, J. and Arnold, C.P. 1990. Computer Analysis of Power System, John Wiley&Sons, New York.

Demello, F.P. and Concordia, C. 1969. Concepts of synchronous machine stability as affected by excitation control. IEEE Trans. Power Appar. Syst., 88: 316-327.

El-Sherbiny, M. and Mehta, D.M. 1973. Dynamic system stability. Part 1: Investigation of the effect of different loading and excitation systems. IEEE Trans. Power Appar. Syst., 92: 212-220.

Padiyar, K.R. 1995. Power System Dynamics Stability and Control, John Wiley & Sons New York.

Saccomanno, F. 2003. Electric Power System Analysis and Control, Wiley-IEEE Press.

Saidy, M. and Hughes, F.M. 1994. Block diagram transfer function model of a generator including damper winding. IEE Proc. Gener. Transm. Distrib., 141: 599-608.

Saidy, M. and Hughes, F.M. 1995. Performance improvement of a conventional power system stabilizer. Int. J. of Electr. Power Energy Syst., 17: 313-323.

Yu, Y. 1983. Electric Power System Dynamic, Academic Press, New York.

Appendix A

System differential and algebraic equations:

$$\frac{d\delta}{dt} = \omega_r - \omega_s \tag{A-1}$$

$$2H\frac{d\omega_r}{dt} = \omega_s(P_m - P_e - K_D(\omega_r - \omega_s)) \tag{A-2}$$

$$\tau'_{do}\frac{dE'_q}{dt} = E_{fd} - E'_q + (X_d - X'_d)I_d \tag{A-3}$$

$$\tau'_{qo}\frac{dE'_d}{dt} = -E'_d - (X_q - X'_q)I_q \tag{A-4}$$

$$P_e = E'_q I_q + E'_d I_d + (X'_d - X'_q)I_d I_q \tag{A-5}$$

$$E_t^2 = E_{td}^2 + E_{tq}^2 \tag{A-6}$$

Where

$$E_{td} = E'_d - X'_q I_q \tag{A-7}$$

$$E_{td} = E'_q + X'_d I_d \tag{A-8}$$

Generator current equation:

From Figure 1, the armature current of the generator in *d*- and *q*-axis frame of reference may be written by,

$$I_d + jI_q = (G - j(1/X_t - B))(E_d + jE_q) + j(1/X_t)e^{j\delta}V_\infty \tag{A-9}$$

Decomposing (A-9) into the *d*- and *q*-axis components (I_d and I_q) by making use of (A-7) and (A-8) gives,

$$I_d = \left\{\frac{G}{Det}\right\}E'_d + \left\{\frac{(1/X_t - B) - (G^2 + (1/X_t - B)^2)X'_q}{Det}\right\}E'_q + V_\infty\left\{\frac{\cos\delta}{X_t Det}\left(1 - (1/X_t - B)X'_q\right) - \frac{G\sin\delta}{X_t Det}X'_q\right\} \tag{A-10}$$

$$I_d = \left\{\frac{G}{Det}\right\}E'_q + \left\{\frac{-(1/X_t - B) + (G^2 + (1/X_t - B)^2)X'_d}{Det}\right\}E'_d + V_\infty\left\{\frac{\sin\delta}{X_t Det}\left(1 - (1/X_t - B)X'_d\right) + \frac{G\cos\delta}{X_t Det}X'_d\right\} \tag{A-11}$$

Where,

$$Det = 1 - (1/X_t - B)(X'_d + X'_q) + (G^2 + (1/X_t - B)^2)X'_d X'_q \tag{A-12}$$

Q-axis transient *e.m.f.* equation:

Substituting (A-10) into (A-3), then linearizing and expressing (A-3) in *s* domain, the *q*-axis transient *e.m.f.* in (3) is obtained with the following coefficients,

$$K_{3q} = \frac{\left\{1+(1/X_t - B)(X_d^{'} + X_q^{'}) + (G^2 + (1/X_t - B)^2)X_d^{'}X_q^{'}\right\}}{\Delta_q^{'}} \tag{A-13}$$

$$K_{4q} = \frac{\left\{V_\infty \sin\delta \frac{(X_d - X_d^{'})}{X_t}(1+(1/X_t - B)X_q^{'}) + V_\infty \cos\delta \frac{G(X_d - X_d^{'})X_q^{'}}{X_t}\right\}}{\Delta_q^{'}} \tag{A-14}$$

$$K_{7q} = \frac{G(X_d - X_d^{'})}{\Delta_q^{'}} \tag{A-15}$$

Where,

$$\Delta_q^{'} = \left\{1+(1/X_t - B)(X_d + X_q^{'}) + (G^2 + (1/X_t - B)^2)X_d X_q^{'}\right\} \tag{A-16}$$

D-axis transient *e.m.f.* equation:

Substituting (A-11) into (A-4), then linearizing and expressing (A-4) in *s* domain, the *d*-axis transient *e.m.f.* in (4) is obtained with the following coefficients,

$$K_{3d} = \frac{\left\{1+(1/X_t - B)(X_d^{'} + X_q^{'}) + (G^2 + (1/X_t - B)^2)X_d^{'}X_q^{'}\right\}}{\Delta_d^{'}} \tag{A-17}$$

$$K_{4d} = \frac{\left\{V_\infty \cos\delta \frac{(X_q - X_q^{'})}{X_t}(1+(1/X_t - B)X_d^{'}) - V_\infty \sin\delta \frac{G(X_q - X_q^{'})X_d^{'}}{X_t}\right\}}{\Delta_d^{'}} \tag{A-18}$$

$$K_{7d} = \frac{G(X_q - X_q^{'})}{\Delta_d^{'}} \tag{A-19}$$

Where,

$$\Delta_d^{'} = \left\{1+(1/X_t - B)(X_q + X_d^{'}) + (G^2 + (1/X_t - B)^2)X_q X_d^{'}\right\} \tag{A-20}$$

Electrical power equation:

Substituting (A-10) and (A-11) into (A-5), and then linearizing and expressing (A-5) in *s* domain, the electrical power of the generator in (5) is obtained with following the coefficients,

$$K_1 = \frac{V_\infty \left\{ (E_q' + (X_d' - X_q')I_d) \begin{pmatrix} \frac{\cos\delta}{X_t}\begin{pmatrix}1+(1/X_t\\ -B)X_d'\end{pmatrix} \\ -\frac{\sin\delta}{X_t}GX_d' \end{pmatrix} - (E_d' + (X_d' - X_q')I_q \begin{pmatrix} \frac{\sin\delta}{X_t}\begin{pmatrix}1+(1/X_t\\ -B)X_q'\end{pmatrix} \\ +\frac{\cos\delta}{X_t}GX_q' \end{pmatrix} \right\}}{\Delta_{dq}'}$$

(A-21)

$$K_{2q} = I_q + \frac{\left(-(E_d' + (X_d' - X_q')I_q) \begin{pmatrix} (1/X_t - B) + (1/X_t \\ -B)^2 X_q' + G^2 X_q' \end{pmatrix} + G(E_q' + (X_d' - X_q')I_d) \right)}{\Delta_{dq}'} \quad \text{(A-22)}$$

$$K_{2d} = I_d + \frac{\left(-(E_q' + (X_d' - X_q')I_d) \begin{pmatrix} (1/X_t - B) + (1/X_t \\ -B)^2 X_d' + G^2 X_d' \end{pmatrix} + G(E_d' + (X_d' - X_q')I_q) \right)}{\Delta_{dq}'} \quad \text{(A-23)}$$

Where,

$$\Delta_{dq}' = \{1 + (1/X_t - B)(X_q' + X_d') + (G^2 + (1/X_t - B)^2 X_q' X_d'\} \quad \text{(A-24)}$$

Terminal voltage equation:

Substituting (A-10) and (A-11) into (A-6), and then linearizing and expressing (A-6) in *s* domain, the terminal voltage of synchronous generator in (6) is obtained with the following coefficients,

$$K_5 = \frac{V_\infty \left\{ \frac{E_{td}}{E_t} X_q' \left(\frac{\sin\delta}{X_t} GX_d' - \frac{\cos\delta}{X_t}\begin{pmatrix}1+(1/X_t\\ -B)X_d'\end{pmatrix} \right) - \frac{E_{tq}}{E_t} X_d' \left(\frac{\cos\delta}{X_t} GX_q' + \frac{\sin\delta}{X_t}\begin{pmatrix}1+(1/X_t\\ -B)X_q'\end{pmatrix} \right) \right\}}{\Delta_{dq}'}$$

(A-25)

$$K_{6q} = \frac{\frac{E_{tq}}{E_t}\{\Delta_{dq}' - X_d'((1/X_t - B) + (G^2 + (1/X_t - B)^2)X_q')\} - \left\{ \frac{E_{td}}{E_t} GX_q' \right\}}{\Delta_{dq}'} \quad \text{(A-26)}$$

$$K_{6d} = \frac{\frac{E_{td}}{E_t}\{\Delta_{dq}' - X_q'((1/X_t - B) + (G^2 + (1/X_t - B)^2)X_d')\} - \left\{ \frac{E_{tq}}{E_t} GX_d' \right\}}{\Delta_{dq}'} \quad \text{(A-27)}$$

Appendix B

160MVA synchronous generator parameters

X_d = 1.700 pu, X_q = 1.640 pu, X'_d = 0.245 pu, X'_q = 0.380 pu,

τ'_{do} = 5.90 sec, τ'_{qo} = 0.54 sec, H = 5.22 sec, K_D = 0.0, f = 60 Hz

(All parameters are based on the generator MVA rating)

AVR parameters

K_a = 200, τ_a = 1.0 sec

Tie line system parameter

X_t = 0.6 pu